

A Disk Census for Young Brown Dwarfs

Ray Jayawardhana

Department of Astronomy, University of Michigan, 830 Dennison Building, Ann Arbor, MI 48109, U.S.A.

David R. Ardila

Bloomberg Center for Physics and Astronomy, Johns Hopkins University, 3400 N. Charles Street, Baltimore, MD 21218, U.S.A.

Beate Stelzer

Osservatorio Astronomico di Palermo, Piazza del Parlamento 1, I-90134 Palermo, Italy

and

Karl E. Haisch, Jr.

Department of Astronomy, University of Michigan, 830 Dennison Building, Ann Arbor, MI 48109, U.S.A.

ABSTRACT

Recent surveys have identified sub-stellar objects down to planetary masses in nearby star-forming regions. Reliable determination of the disk frequency in young brown dwarfs is of paramount importance to understanding their origin. Here we report the results of a systematic study of infrared L' -band ($3.8\mu\text{m}$) disk excess in ~ 50 spectroscopically confirmed objects near and below the sub-stellar boundary in several young clusters. Our observations, using the ESO Very Large Telescope, Keck I and the NASA Infrared Telescope Facility, reveal that a significant fraction of brown dwarfs harbor disks at a very young age. Their inner disk lifetimes do not appear to be vastly different from those of disks around T Tauri stars. Our findings are consistent with the hypothesis that sub-stellar objects form via a mechanism similar to solar-mass stars.

Subject headings: stars: low mass, brown dwarfs – stars: pre-main-sequence – circumstellar matter – planetary systems – stars: formation

1. Introduction

The current paradigm of low-mass star formation holds that a young star accretes material from a circumstellar disk during the first (few) million years of its lifetime. The disk also provides the building material for planets. Over the past two decades, substantial observational evidence has accumulated to support this picture. However, much of that evidence rests on studies of stars within a relatively narrow mass range. In particular, there are few observational constraints on the formation of objects near or below the sub-stellar boundary.

The past five years have seen the detection of a large number of sub-stellar objects in the solar neighborhood and in young clusters. Large-scale optical and near-infrared surveys of the sky –such as the Sloan Digital Sky Survey and the 2-Micron All-Sky Survey (2MASS)– have turned up (older) field brown dwarfs with L and T spectral types (e.g., Kirkpatrick et al. 2000; Fan et al. 2000). Meanwhile, their young counterparts have been identified in star-forming regions through more targeted searches (e.g., Luhman et al. 2000; Ardila, Martín & Basri 2000). Perhaps the most surprising of recent findings has been the discovery of a population of young, isolated planetary mass objects –or “planemos”– in the σ Orionis (Zapatero-Osorio et al. 2000), Trapezium (Lucas & Roche 2000) and Upper Scorpius (Mohanty, Jayawardhana & Basri 2003) regions.

Still, the formation mechanism for brown dwarfs is open to debate. Reipurth & Clarke (2001) and Bate et al. (2002) have proposed that brown dwarfs are stellar embryos, ejected from newborn multiple systems before they can accrete sufficient mass for hydrogen fusion. Padoan & Nordlund (2003), on the other hand, have suggested that brown dwarfs form in the same way as more massive stars, via ‘turbulent fragmentation’.

Studies of disks around young brown dwarfs provide one of the few observational probes to distinguish among these scenarios. If a substantial fraction of brown dwarfs harbor large, long-lived accretion disks, the implication is that extremely low-mass objects may form via a mechanism similar to higher mass stars. Thus, reliable determination of the disk frequency and lifetime in young brown dwarfs is of paramount importance to our understanding of the origin and diversity of sub-stellar objects down to planetary masses. In a pioneering study, Muench et al. (2001) reported that $65\% \pm 15\%$ of brown dwarf *candidates* in the Trapezium cluster exhibit JHK colors consistent with circumstellar disks.

Here we report on a systematic study of infrared L' -band ($3.8\mu\text{m}$) disk excess in a large sample of *spectroscopically confirmed* objects near and below the sub-stellar boundary in several nearby star-forming regions. Our longer-wavelength observations are much better at detecting disk excess above the photospheric emission and are less susceptible to the effects

of disk geometry and extinction corrections than *JHK* studies (e.g., Haisch, Lada & Lada 2001; Liu, Najita & Tokunaga 2003).

2. Observations

Our target sample consists of very low mass (VLM) objects with known spectral types later than M5 in nearby star-forming regions. They are drawn from surveys of ρ Ophiuchus (Wilking, Greene & Meyer 1999), IC 348 (Luhman 1999), Chamaeleon I (Comerón, Neuhäuser & Kaas 2000; Comerón, Rieke & Neuhäuser 1999), Taurus (Briceño et al. 2002), Upper Scorpius (Ardila, Martín & Basri 2000), σ Orionis (Béjar, Zapatero Osorio & Rebolo 1999), and the TW Hydrae Association (Gizis 2002).

Observations were carried out at three different telescopes during 2002. Table 1 provides a summary log. When *JHK* magnitudes were not available in the literature or in the 2MASS database, we also obtained photometric observations in those filters. The transformations between the different photometric systems are smaller than the measuring errors (Carpenter 2001).

The observations at the Very Large Telescope (VLT) were obtained in service mode using the Infrared Spectrograph and Array Camera (ISAAC; Moorwood et al. 1998). At Keck I, we used the Near InfraRed Camera (NIRC; Matthews & Soifer 1994). *JHK* data were obtained in a five-point pattern. The L' -band data were acquired in the chop-nod mode (15 to 30" offsets), in order to cancel out the variable thermal background. Each observation consisted of a large number of co-added frames with short exposure times. Observations of several ρ Oph sources were obtained with the NSFCAM camera (Rayner et al. 1993; Shure et al. 1994) on the NASA InfraRed Telescope Facility (IRTF). Each source was observed in a five point dither pattern. At each dither position, the telescope was nodded to separate sky positions 30" of the target observation.

All the data were reduced using standard tools within the Image Reduction and Analysis Facility (IRAF)¹. Flat fields were obtained by combining individual images. For the *JHK* observations the sky was subtracted from each frame. Aperture photometry was performed for each source, using the PHOT routine within IRAF. The standards were observed on the same nights and through the same range of airmasses as the target sources.

¹IRAF is distributed by the National Optical Astronomy Observatories, which are operated by the Association of Universities for Research in Astronomy, Inc., under cooperative agreement with the National Science Foundation.

Zero points and extinction coefficients were established for each night. The photometric accuracy of our observations are typically ± 0.10 magnitudes, though in a few cases they can be ± 0.20 magnitudes.

3. Results and Discussion

Table 2 lists the $JHKL'$ magnitudes and $J - H, H - K, K - L'$ colors of our targets. Figure 1 shows their $K - L'$ colors as a function of spectral type in comparison to the locus of field M dwarfs from Leggett et al. (2002). It is clear that a significant fraction of our targets have redder $K - L'$ colors than would be expected from photospheric emission alone. The lower envelope of their color distribution does agree reasonably well with the field M dwarf locus.

In Figure 2, we plot the $J - H/K - L'$ color-color diagram for our target sample. For comparison, we also plot the empirical loci of colors for giants and for main-sequence dwarfs from Bessell & Brett (1988) and Leggett et al. (2002). Again, we find that a large fraction of our sources fall to the right of the reddening band for M dwarfs and into the infrared excess region of the color-color diagram.

Since all objects in our sample have known spectral types, we can determine their intrinsic photospheric $K - L'$ by comparison to field M dwarfs of the same type and by using a reddening law (e.g., Cohen et al. 1981). An excess of $K - L' \gtrsim 0.2$ above the stellar photosphere is usually indicative of an optically thick disk around a late-type object and is also a reasonable criterion given the typical photometric errors in our data as well as possible color differences in field objects due to higher gravity/older age. Table 3 lists the spectral types and $K - L'$ excesses of our targets, along with the equivalent width of their $H\alpha$ emission, when available in the literature. Table 4 gives the infrared excess fraction in each star-forming region.

Of the seven ρ Ophiuchus objects for which we have L' photometry, four exhibit $K - L'$ excesses. Two other objects on our target list –GY 11 and GY 141– which we could not observe at L' also show evidence of optically thick disks according to the Infrared Space Observatory (ISO) measurements at $6.7\mu\text{m}$ and $14.3\mu\text{m}$ (Testi et al. 2002; Comerón et al. 1998). The high disk fraction among ρ Oph brown dwarfs is not surprising, given that ρ Oph is the most embedded, and probably the youngest, cluster in our survey at an age of $\lesssim 1$ Myr. Our finding is also consistent with that of Natta et al. (2002) who reported ISO-detected mid-infrared excess in nine other VLM sources in this region. These authors were able to fit the excesses with irradiated disk models.

We find disk fractions of 40%–60% in IC 348, Chamaeleon I, Taurus and Upper Scorpius regions. Based on ISO observations, Natta & Testi (2001) have already shown that Cha H α 1, ChaH α 2 and ChaH α 9 harbor mid-infrared spectral energy distributions consistent with the presence of dusty disks. ChaH α 2, which shows a large $K - L'$ excess (0.97 mag) in our data is a probable close ($\sim 0.2''$) binary with roughly equal-mass companions (Neuhäuser et al. 2002). It is possible that a few of our targets harbor infrared companions that contribute to the measured excess, but this is unlikely in most cases. The disk fractions we report for IC 348 and Taurus are lower than those found by Liu, Najita & Tokunaga (2003). This is primarily because we use a more conservative criterion of $K - L' > 0.2$ for the presence of optically thick disks whereas Liu et al. consider all objects with $K - L' > 0$ as harboring disks. In both these regions, our disk fractions are comparable to those derived from H α accretion signatures in high-resolution optical spectra (Jayawardhana, Mohanty & Basri 2003; White & Basri 2002). However, in Upper Sco, which may be slightly older at $\sim 3\text{--}5$ Myrs, we find $K - L'$ excess in $\sim 50\%$ of the targets whereas only one out of 11 VLM objects exhibit accretion-like H α (Jayawardhana, Mohanty & Basri 2002; 2003). This latter result suggests that dust disks may persist after accretion has ceased or been reduced to a trickle, as also suggested by Haisch, Lada & Lada (2001).

In the somewhat older (~ 5 Myr) σ Orionis cluster, only about a third of the targets show infrared excess. Neither of the two brown dwarf candidate members of the ~ 10 -Myr-old TW Hydreae association (Gizis 2002) shows excess. Gizis (2002) reported strong H α emission (equivalent width ≈ 300 Å) from one of the TW Hydreae objects, the M8 dwarf 2MASSW J1207334-393254, and suggested it could be due to either accretion or chromospheric activity. Given the lack of measurable $K - L'$ excess in this object, accretion now appears less likely as the cause of its strong H α emission. Our findings in σ Ori and TW Hya associations, albeit for a small sample of objects, could mean that the inner disks are clearing out by the age of these groups. Similar results have been found for T Tauri stars in the TW Hydreae association (Jayawardhana et al. 1999).

Jayawardhana, Mohanty & Basri (2003) report a decrease in the fraction of accreting brown dwarfs with increasing age in a study of H α line profiles in high-resolution optical spectra. This trend is in general agreement with our results here based on infrared excess measurements. However, as shown in Figure 3, we do not find a one-to-one correlation between objects with $K - L'$ excess and those with large H α equivalent widths. As mentioned earlier, several of the Upper Sco VLM objects with excess do not exhibit accretion-like H α . While this is somewhat surprising, it is not unprecedented. For example, in IC 348, Haisch, Lada, & Lada (2001) found that 10/17 weak-line (H α EW < 10 Å) T Tauri stars in their sample showed $K - L'$ excess. Persistence of disks after the accretion rates have significantly diminished could explain these results. Another complication is that

the H α equivalent widths in Table 3 are drawn from a variety of sources in the literature. Many of the measurements have been made with low- or medium-resolution spectra. It has been shown that low-resolution spectra of late-type objects systematically overestimate the H α equivalent width as a result of blending with the 6569Å TiO band-head (e.g., Tinney & Reid 1998). This effect can confuse the relation between H α width and infrared excess.

4. Concluding Remarks

Our results, and those of Muench et al. (2001), Natta et al. (2002), and Liu, Najita & Tokunaga (2003) show that a large fraction of very young brown dwarfs harbor near- and mid-infrared excesses consistent with dusty disks. High-resolution optical spectra have revealed accretion signatures in many sources (Jayawardhana, Mohanty & Basri 2003). Taken together, the evidence is compelling that sub-stellar objects are surrounded by accretion disks similar to those around T Tauri stars, possibly less massive. While the samples are still relatively small, the timescales for inner disk depletion do not appear to be vastly different between brown dwarfs and T Tauri stars (whereas Armitage & Clarke 1997, for example, predict faster disk evolution for ejected objects). Therefore, the evidence to date is consistent with a common formation scenario for low-mass stars and brown dwarfs. Far-infrared observations with the *Space InfraRed Telescope Facility* and/or the *Stratospheric Observatory For Infrared Astronomy* will be crucial for deriving the sizes of circum-sub-stellar disks and providing a more definitive test of the ejection hypothesis for the origin of brown dwarfs.

We thank Geoff Marcy for useful discussions, constant encouragement and access to Keck and Kevin Luhman for valuable assistance during the December 2002 Keck run. We are grateful to the staff members of the VLT, Keck and IRTF observatories for their outstanding support. We also thank Fernando Comerón and staff at the ESO User Support Group for their prompt responses to our queries. We would like to acknowledge the great cultural significance of Mauna Kea for native Hawaiians, and express our gratitude for permission to observe from its summit. This work was supported in part by NSF grant AST-0205130 and NASA grant NAG5-13136 to R.J.

REFERENCES

Ardila, D., Martín, E., & Basri, G. 2000, AJ, 120, 479
Armitage, P.J. & Clarke, C.J. 1997, MNRAS 285, 540

Bate, M. R., Bonnell, I. A. & Bromm, V. 2002, MNRAS, 336, 705

Béjar V. J. S., Zapatero Osorio, M. R. & Rebolo, R. 1999, ApJ, 521, 671

Béjar V. J. S., et al. 2001, ApJ, 556, 830

Bessell, M. S. & Brett, J. M. 1988, PASP, 100, 1134

Briceño, C., et al. 2002, ApJ, 580, 317

Carpenter, J. 2001, AJ, 121, 2851

Cohen, J.G., Frogel, J.A., Persson, S.E., & Elias, J.H. 1981, ApJ, 249, 481

Comerón, F., et al. 1998, A&A, 335, 522

Comerón, F., Rieke, G. H. & Neuhäuser, R. 1999, A&A, 343, 477

Comerón, F., Neuhäuser, R. & Kaas, A. A. 2000, A&A, 359, 269

Fan, X., et al. 2000, AJ, 119, 928

Gizis, J.E. 2002, ApJ, 575, 484

Haisch, K. E. Jr., Lada, E. A. & Lada, C. J. 2001, AJ, 121, 2065

Jayawardhana, R., et al. 1999, ApJ, 521, L129

Jayawardhana, R., Mohanty, S., & Basri, G. 2002, ApJ, 578, L141

Jayawardhana, R., Mohanty, S., & Basri, G. 2003, ApJ, in press

Kirkpatrick, D., et al. 2000, AJ, 120, 447

Leggett, S. K., et al. 2002, ApJ, 564, 452

Liu, M. C., Najita, J. & Tokunaga, A. T. 2003, ApJ, 585, 372

Lucas, P. W. & Roche, P. F. 2000, MNRAS, 314, 858

Luhman, K. L. & Rieke, G.H. 1999, ApJ, 525, 440

Luhman, K. L. 1999, ApJ, 525, 466

Luhman, K. L., et al. 2000, ApJ, 540, 1016

Matthews, K. & Soifer, B. T. 1994, Experimental Astronomy, vol. 3, No. 1-4, 77

Mohanty, S., Jayawardhana R., & Basri, G. 2003, ApJ, submitted

Moorwood, A., et al. 1998, ESO Messenger, 94, 7

Muench, A.A., et al. 2001, ApJ, 558, L51

Natta, A. & Testi, L. 2001, A&A, 376, L22

Natta, A., et al. 2002, A&A, 393, 597

Neuhäuser, R., et al. 2002, A&A, 384, 999
Padoan, P. & Nordlund, A. 2003, ApJ, in press
Rayner, J. T., et al. 1993, Proc. SPIE, 1946, 490
Reipurth, B. & Clarke, C. 2001, AJ, 122, 432
Shure M. A., et al. 1994, Proc. SPIE, 2198, 614
Testi, L., et al. 2002, ApJ, 571, L155
Tinney, C. G. & Reid, I. N. 1998, MNRAS, 301, 1031
White, R. J., & Basri, G. 2003, ApJ, 582, 1109
Wilking, B.A., Greene, T.P., & Meyer, M.R. 1999, AJ, 117, 469
Zapatero Osorio, M. R., et al. 2000, Science, 290, 103

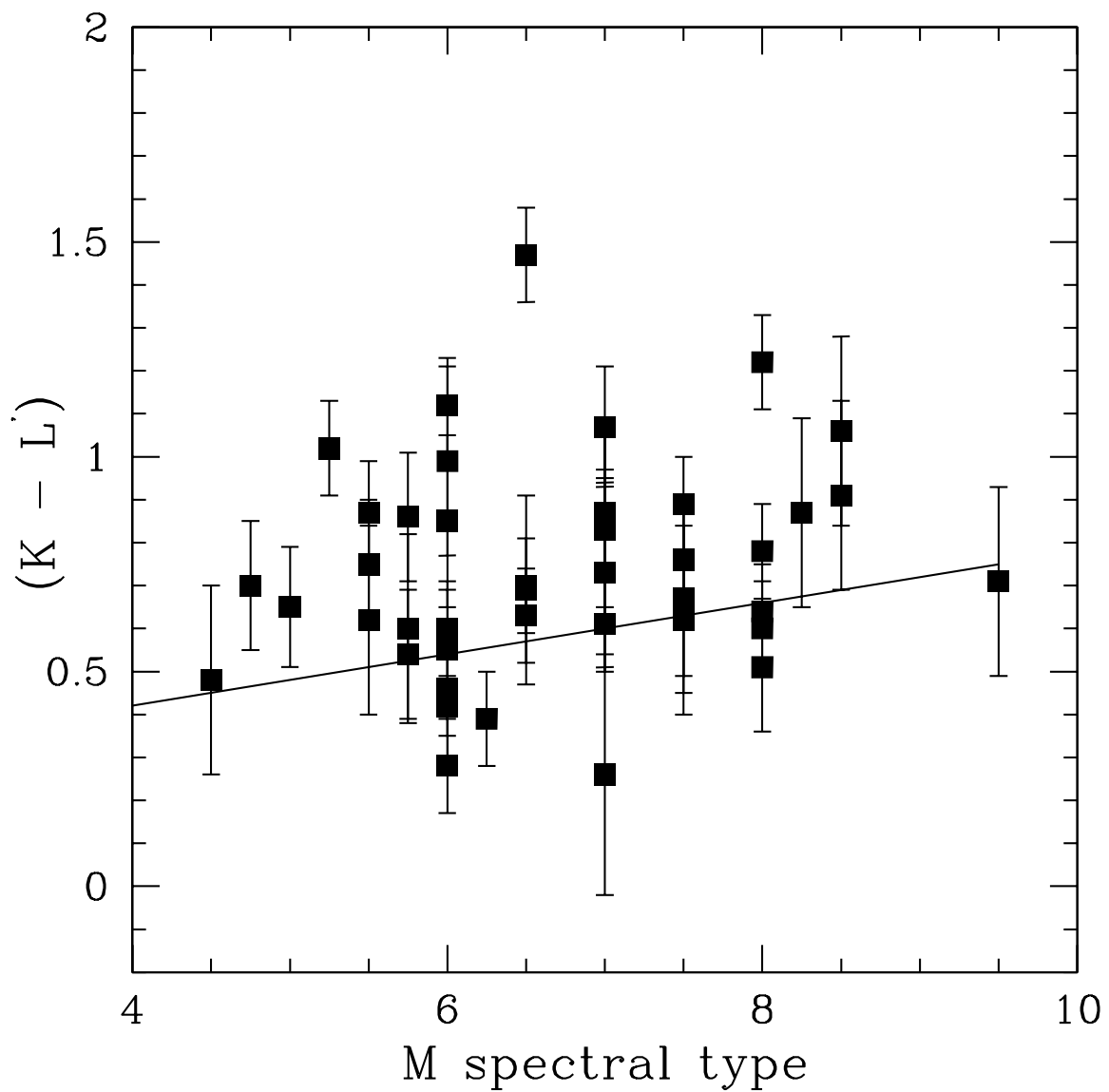


Fig. 1.— $K - L'$ color as a function of spectral type.

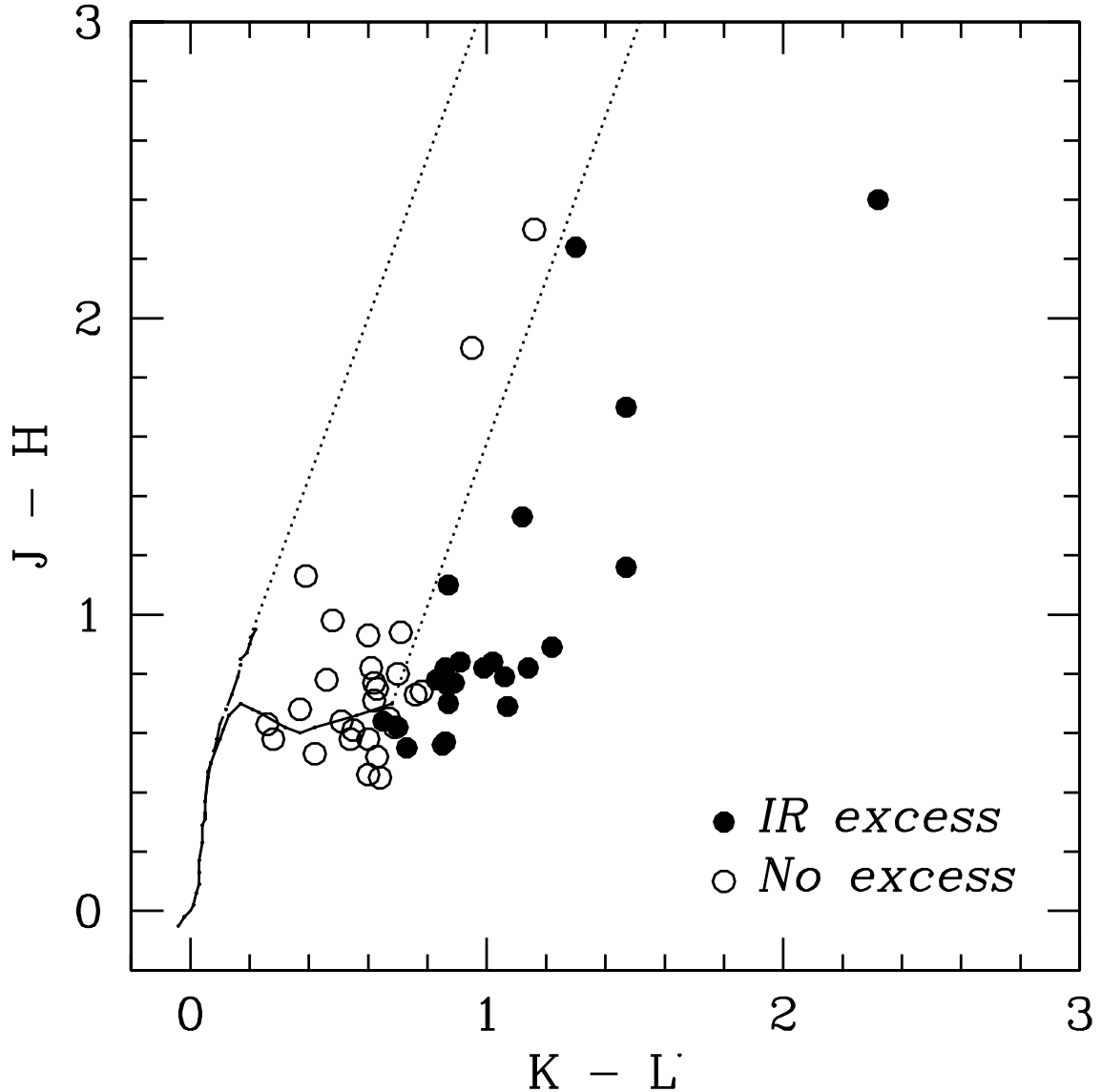


Fig. 2.— $J - H/K - L'$ color-color diagram for our target sample. Also plotted are the empirical loci of colors for giants (solid) and for main-sequence dwarfs (dashed) from Bessell & Brett (1988) and Leggett et al. (2002) and the reddening vectors (dotted). The filled circles are stars with $E(K - L') > 0.2$.

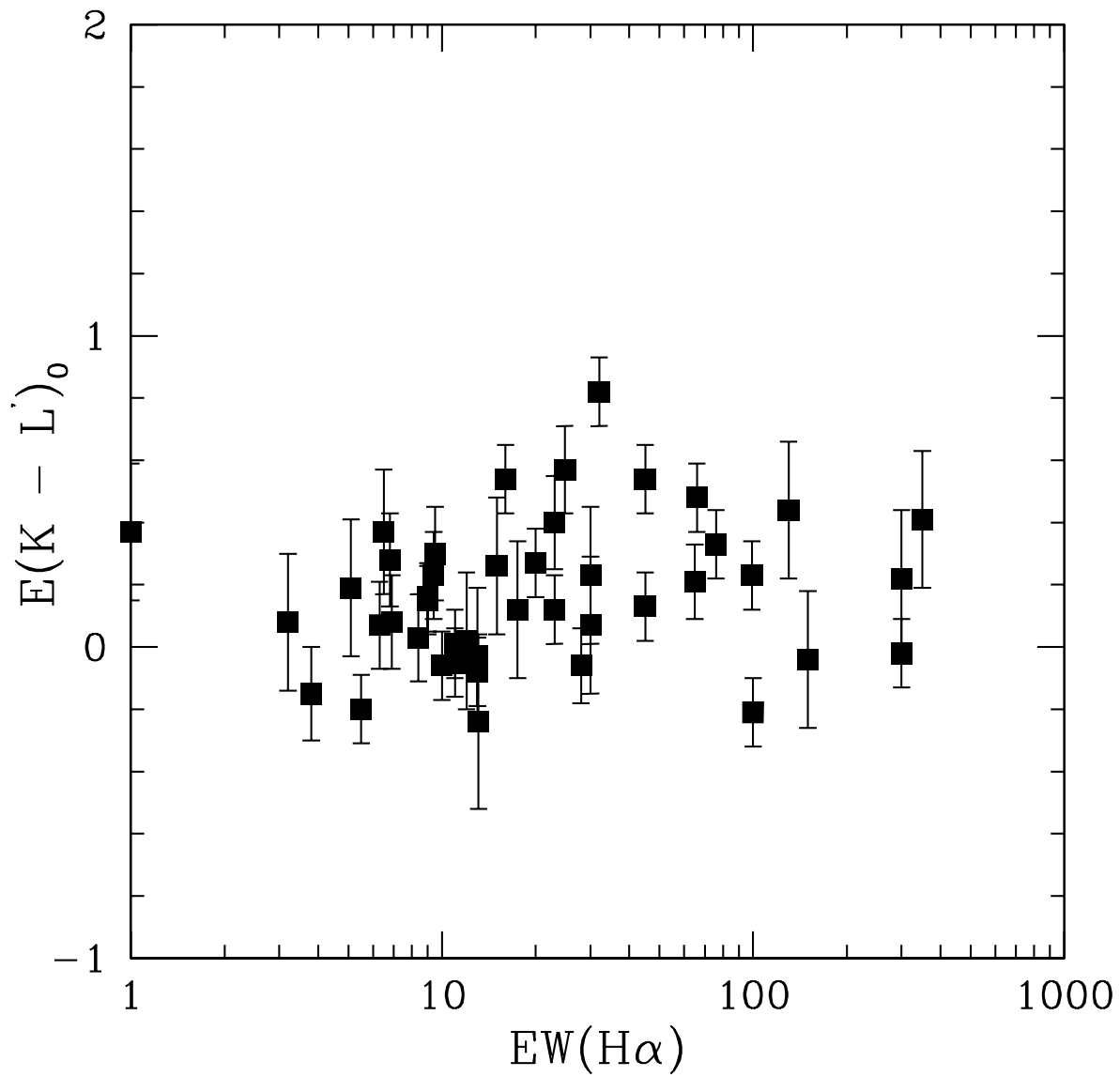


Fig. 3.— Relation between $K - L'$ excess and equivalent width of $H\alpha$ emission in Angstroms, from the literature, as listed in Table 3.

Table 1. Log of Observations

UT Date	Telescope	Target	Filter	On-Source Integration (s)	Flux Standard
2002 January 11	VLT-ANTU	S Ori 12	L'	240	HR4638
		S Ori 17	L'	720	HR4638
		S Ori 25	L'	1080	HR4638
		S Ori 29	L'	780	HR4638
		S Ori 39	L'	1860	HR4638
		S Ori 40	L'	1320	HR4638
2002 April 15	VLT-ANTU	Cha H α 1	L'	118.8	HD83844
		Cha H α 2	L'	118.8	HD83844
		Cha H α 3	L'	118.8	HD83844
		Cha H α 4	L'	118.8	HD83844
		Cha H α 5	L'	118.8	HD83844
		Cha H α 6	L'	118.8	HD83844
		Cha H α 7	L'	118.8	HD83844
		Cha H α 8	L'	118.8	HD83844
		Cha H α 9	L'	118.8	HD83844
		Cha H α 10	L'	297	HD83844
		Cha H α 11	L'	594	HD83844
		Cha H α 12	L'	118.8	HD83844
2002 April 20	VLT-ANTU	UScoCTIO 104	L'	118.8	HD130163
		UScoCTIO 109	L'	237.6	HD130163
		UScoCTIO 128	L'	415.8	HD130163
2002 April 23	Keck I	GY 202	K	6	HD129655
			L'	10	HD129655
2002 April 24	Keck I	UScoCTIO 112	K	35	LHS2397a
			L'	60	LHS2397a
		UScoCTIO 130	K	35	LHS2397a
			L'	300	LHS2397a
		UScoCTIO 137	K	10	LHS2397a
			L'	300	LHS2397a
		2MASSW J1207334-393254	J	25	LHS2397a
			H	25	LHS2397a
2002 May 30	VLT-ANTU		K	35	LHS2397a
			L'	40	LHS2397a
		2MASSW J1139511-315921	J	50	LHS2397a
			H	50	LHS2397a
			K	35	LHS2397a
			L'	40	LHS2397a
		UScoCTIO 100	J	80	S860-D
			H	80	S860-D
			K	80	S860-D
		UScoCTIO 104	J	80	S860-D

Table 1—Continued

UT Date	Telescope	Target	Filter	On-Source Integration (s)	Flux Standard	
2002 June 12	VLT-ANTU	UScoCTIO 109	H	80	S860-D	
			K	80	S860-D	
		UScoCTIO 128	J	80	S860-D	
			H	80	S860-D	
		UScoCTIO 132	K	80	S860-D	
			K	80	S860-D	
		CHXR 78c	K	80	S860-D	
			J	80	S860-D	
		CHXR 73	H	80	S860-D	
			K	80	S860-D	
2002 June 13	VLT-ANTU	CHXR 74	L'	118.8	S587-T	
			L'	118.8	S587-T	
		Cha H α 12	L'	118.8	S860-D	
			J	80	S860-D	
		Cha H α 12	H	80	S860-D	
			K	80	S860-D	
		Cha H α 8	J	80	S860-D	
			H	80	S860-D	
			K	80	S860-D	
		CRBR 14	J	25	HD161903	
2002 June 15	IRTF		H	25	HD161903	
			K	25	HD161903	
			L'	25	HD161903	
	CRBR 15	J	25	HD161903		
		H	25	HD161903		
	GY 5	K	25	HD161903		
		L'	25	HD161903		
	GY 10	J	25	HD161903		
		H	25	HD161903		
	GY 59	K	25	HD161903		
		L'	25	HD161903		
	GY 64	J	25	HD161903		
		H	25	HD161903		

Table 1—Continued

UT Date	Telescope	Target	Filter	On-Source Integration (s)	Flux Standard
			K	25	HD161903
			L'	25	HD161903
2002 August 12	VLT-ANTU	UScoCTIO 132	L'	475.2	HR6070
2002 December 19	Keck I	IC348 165	K	5	GD50
			L'	20	HD22686
		IC348 256	K	5	GD50
			L'	20	HD22686
		IC348 286	K	5	GD50
			L'	100	HD22686
		IC348 363	K	5	GD50
			L'	400	HD22686
		IC348 367	K	5	GD50
			L'	400	HD22686
		IC348 478	K	5	GD50
			L'	400	HD22686
2002 December 20	Keck I	KPNO-Tau 1	L'	200	HD22686
		KPNO-Tau 2	L'	80	HD22686
		KPNO-Tau 3	L'	20	HD22686
		KPNO-Tau 4	L'	200	HD22686
		KPNO-Tau 5	L'	20	HD22686
		KPNO-Tau 6	L'	200	HD22686
		KPNO-Tau 7	L'	200	HD22686
		KPNO-Tau 8	L'	20	HD22686
		KPNO-Tau 9	L'	600	HD22686

Table 2. Positions and $JHKL'$ Magnitudes and Colors

Source	RA(J2000)	Dec(J2000)	J ^a	H ^a	K ^a	L'	(J-H)	(H-K)	(K-L')
IC348 165	03 44 35.43	+32 08 54.4	13.15	12.31	11.84	10.82	0.84	0.47	1.02
IC348 256	03 43 55.14	+32 07 55.0	13.59	13.02	12.54	11.68	0.57	0.48	0.86
IC348 286	03 45 06.80	+32 09 26.8	13.76	13.18	12.71	12.17	0.58	0.47	0.54
IC348 363	03 44 17.00	+32 00 15.3	14.83	14.19	13.80	13.29	0.64	0.39	0.51
IC348 367	03 43 59.03	+32 05 57.9	14.72	14.10	13.59	12.89	0.62	0.51	0.70
IC348 478	03 44 35.97	+32 11 15.9	16.17	15.04	14.60	14.21	1.13	0.44	0.39
KPNO-Tau 1	04 15 14.72	+28 00 09.5	15.09	14.25	13.74	12.83	0.84	0.51	0.91
KPNO-Tau 2	04 18 51.15	+28 14 33.3	13.89	13.18	12.74	12.12	0.71	0.44	0.62
KPNO-Tau 3	04 26 29.38	+26 24 14.2	13.32	12.50	12.08	11.09	0.82	0.42	0.99
KPNO-Tau 4	04 27 28.01	+26 12 05.3	14.98	14.04	13.31	12.60	0.94	0.73	0.71
KPNO-Tau 5	04 29 45.68	+26 30 46.7	12.61	11.96	11.50	10.83	0.65	0.46	0.67
KPNO-Tau 6	04 30 07.25	+26 08 20.7	15.00	14.21	13.66	12.60	0.79	0.55	1.06
KPNO-Tau 7	04 30 57.21	+25 56 40.0	14.50	13.80	13.22	12.35	0.70	0.58	0.87
KPNO-Tau 8	04 35 41.85	+22 34 11.6	12.96	12.38	12.00	11.40	0.58	0.38	0.60
KPNO-Tau 9	04 35 51.43	+22 49 11.9	15.49	14.67	14.17	13.03	0.82	0.50	1.14
S Ori 12	05 37 57.40	-02 38 45.0	14.20	13.64	13.28	12.43	0.56	0.36	0.85
S Ori 17	05 39 04.40	-02 38 35.0	14.77	14.19	13.79	13.51	0.58	0.40	0.28
S Ori 25	05 39 08.80	-02 39 58.0	14.67	14.15	13.76	13.13	0.52	0.39	0.63
S Ori 29	05 38 29.50	-02 25 17.0	14.83	14.30	13.96	13.54	0.53	0.34	0.42
S Ori 39	05 38 32.40	-02 29 58.0	15.47	14.85	14.43	13.74	0.62	0.42	0.69
S Ori 40	05 37 36.40	-02 41 57.0	15.49	14.94	14.59	13.86	0.55	0.35	0.73
Cha H α 1	11 07 17.00	-77 35 54.0	13.55	12.78	12.28	11.39	0.77	0.50	0.89
Cha H α 2	11 07 43.00	-77 33 59.0	12.59	11.43	11.15	9.68	1.16	0.28	1.47
Cha H α 3	11 07 52.90	-77 36 56.0	12.46	11.64	11.11	10.50	0.82	0.53	0.61
Cha H α 4	11 08 19.60	-77 39 17.0	12.20	11.42	11.04	10.58	0.78	0.38	0.46
Cha H α 5	11 08 25.60	-77 41 46.0	12.14	11.21	10.76	10.16	0.93	0.45	0.60
Cha H α 6	11 08 40.20	-77 34 17.0	12.43	11.61	11.09	10.23	0.82	0.52	0.86
Cha H α 7	11 07 38.40	-77 35 30.0	13.89	13.00	12.51	11.29	0.89	0.49	1.22
Cha H α 8	11 07 47.80	-77 40 08.0	12.92	12.12	11.63	10.93	0.80	0.49	0.70
Cha H α 9	11 07 19.20	-77 32 52.0	13.92	12.59	11.82	10.70	1.33	0.77	1.12
Cha H α 10	11 08 25.60	-77 39 30.0	14.41	13.68	13.27	12.51	0.73	0.41	0.76
Cha H α 11	11 08 30.80	-77 39 19.0	14.72	13.98	13.57	12.79	0.74	0.41	0.78
Cha H α 12	11 06 37.50	-77 43 07.0	13.20	12.42	12.00	11.17	0.78	0.42	0.83
CHXR 73	11 06 28.90	-77 37 33.0	13.00	11.32	10.79	10.11	1.68	0.53	0.68
CHXR 74	11 06 57.40	-77 42 10.4	11.55	10.57	10.23	9.75	0.98	0.34	0.48
CHXR 78C	11 08 54.60	-77 32 12.0	12.41	11.64	11.28	10.66	0.77	0.36	0.62
Gizis 1	11 39 51.10	-31 59 21.0	12.62	12.16	11.57	10.97	0.46	0.59	0.60
Gizis 2	12 07 33.40	-39 32 54.0	13.02	12.57	12.02	11.38	0.45	0.55	0.64
UScoCTIO 100	16 02 04.13	-20 50 41.5	12.83	12.20	11.78	11.52	0.63	0.42	0.26
UScoCTIO 104	15 57 12.66	-23 43 45.3	13.52	12.88	12.52	11.87	0.64	0.36	0.65
UScoCTIO 109	16 01 19.10	-23 06 38.6	13.64	13.03	12.66	12.11	0.61	0.37	0.55

Table 2—Continued

Source	RA(J2000)	Dec(J2000)	J ^a	H ^a	K ^a	L'	(J-H)	(H-K)	(K-L')
UScoCTIO 112	16 00 26.57	-20 56 32.0			12.81	12.06			0.75
UScoCTIO 128	15 59 11.20	-23 37 59.0	14.41	13.72	13.27	12.20	0.69	0.45	1.07
UScoCTIO 130	15 59 43.56	-20 14 38.1	14.29	13.54	13.12	12.49	0.75	0.42	0.63
UScoCTIO 132	15 59 37.74	-22 54 09.5	14.31	13.55	13.08	12.21	0.76	0.47	0.87
UScoCTIO 137	15 56 47.87	-23 47 44.0	15.60	14.92	14.41	14.04	0.68	0.51	0.37
CRBR 14	16 26 19.07	-24 26 12.0	15.20	13.50	12.34	10.87	1.70	1.16	1.47
CRBR 15	16 26 19.05	-24 24 16.8	16.30	13.90	11.94	9.62	2.40	1.96	2.32
GY 5	16 26 21.70	-24 26 02.0	12.70	11.60	10.94	10.07	1.10	0.66	0.87
GY 10	16 26 22.30	-24 23 54.0	15.80	13.50	12.24	11.08	2.30	1.26	1.16
GY 11	16 26 22.40	-24 24 08.0	16.50	15.40	14.15		1.10	1.25	
GY 59	16 26 31.30	-24 25 32.0	14.70	12.80	11.68	10.73	1.90	1.12	0.95
GY 64	16 26 32.60	-24 26 38.0	16.50	14.70	13.34	> 12.80	1.80	1.36	< 0.54
GY 141	16 26 51.40	-24 32 44.0	15.10	14.40	13.90		0.70	0.50	
GY 202	16 27 06.00	-24 28 36.0	16.76	14.52	13.01	11.71	2.24	1.51	1.30

^a*J, H* magnitudes for IC 348 sources from Luhman (1999), *J, H, K* magnitudes for Taurus sources from Briceño et al. (2002), *J, H, K* magnitudes for Chamaeleon sources 1 - 7, and 9 - 11 taken from Comerón, Neuhäuser, & Kaas (2000), *J, H* magnitudes for Upper Sco 128, and 130 taken from Ardila, Martín, & Basri (2000).

Table 3. Spectral Type, Infrared Excess, and $W_{\lambda}(\text{H}\alpha)$

Source	ST ^a	$E(K-L')_0$	$W_{\lambda}(\text{H}\alpha)(\text{\AA})^a$
IC348 165	M5.25	0.48	66.0
IC348 256	M5.75	0.40	23.0
IC348 286	M5.75	0.08	6.9
IC348 363	M8	-0.15	3.8
IC348 367	M4.75	0.28	6.8
IC348 478	M6.25	-0.21	100.0
KPNO-Tau 1	M8.5	0.26	15.0
KPNO-Tau 2	M7.5	0.02	12.0
KPNO-Tau 3	M6	0.44	130.0
KPNO-Tau 4	M9.5	-0.04	150.0
KPNO-Tau 5	M7.5	0.07	30.0
KPNO-Tau 6	M8.5	0.41	350.0
KPNO-Tau 7	M8.25	0.22	300.0
KPNO-Tau 8	M5.75	0.12	17.5
KPNO-Tau 9	M8.5	0.49	
S Ori 12	M6	0.37	6.5
S Ori 17	M6	-0.20	5.5
S Ori 25	M6.5	0.13	45.0
S Ori 29	M6	-0.06	28.0
S Ori 39	M6.5	0.19	5.1
S Ori 40	M7	0.23	30.0
Cha H α 1	M7.5	0.23	99.0
Cha H α 2	M6.5	0.82	32.0
Cha H α 3	M7	-0.08	13.0
Cha H α 4	M6	-0.05	11.0
Cha H α 5	M6	0.01	11.0
Cha H α 6	M7	0.33	76.0
Cha H α 7	M8	0.54	45.0
Cha H α 8	M6.5	0.16	9.0
Cha H α 9	M6	0.54	16.0
Cha H α 10	M7.5	0.15	9.0
Cha H α 11	M8	0.12	23.0
Cha H α 12	M7:	0.27	20.0
CHXR 73	M4.5:	-0.02	
CHXR 74	M4.5	-0.03	13.0
CHXR 78C	M5.5	0.08	3.2
Gizis 1	M8	-0.06	10.0
Gizis 2	M8	-0.02	300.0
UScoCTIO 100	M7	-0.24	13.1
UScoCTIO 104	M5	0.23	9.4
UScoCTIO 109	M6	0.07	19.0

Table 3—Continued

Source	ST ^a	E(K-L') ₀	W _λ (Hα)(Å) ^a
UScoCTIO 112	M5.5	0.30	9.5
UScoCTIO 128	M7	0.57	24.8
UScoCTIO 130	M7.5	0.03	8.4
UScoCTIO 132	M7	0.37	<1.0
UScoCTIO 137	M7	-0.13	
CRBR 14	M5.5	0.55	
CRBR 15	M5	1.15	
GY 5	M5.5	0.21	64.9
GY 10	M6.5	0.06	
GY 11	M6.5		
GY 59	M5	0.02	
GY 64	M7	<0.04	
GY 141	M8.5		13.4
GY 202	M6.5	0.21	

^aSpectral types and W_λ(Hα) for IC 348 source 478 taken from Luhman (1999), W_λ(Hα) for remaining IC 348 sources from Jayawardhana, Mohanty, & Basri (2003); spectral types and W_λ(Hα) for Taurus, Sigma Orionis, Chamaeleon, and Upper Sco sources from Briceño et al. (2002), Béjar, Zapatero Osorio, & Rebolo (1999), Comerón, Neuhauser, & Kaas (2000), and Ardila, Martín, & Basri (2000) respectively. Spectral types and W_λ(Hα) for Gizens 1 and 2 from Gizens (2002). Spectral types and W_λ(Hα) for ρ Oph sources from Luhman & Rieke (1999) and Jayawardhana, Mohanty, & Basri (2002) respectively.

Table 4. Disk Fractions for Surveyed Regions

Region	Fraction	Estimated Age
ρ Oph	6/9 (67% \pm 27%)	\lesssim 1 Myr
IC 348	3/6 (50% \pm 29%)	\sim 1 Myr
Taurus	5/9 (56% \pm 25%)	\sim 1-3 Myr
Cha I	6/15 (40% \pm 16%)	\sim 1-3 Myr
Upper Sco	4/8 (50% \pm 25%)	\sim 3-5 Myr
σ Ori	2/6 (33% \pm 24%)	\sim 5-7 Myr
TW Hya	0/2	\sim 10 Myr